Plasma Phys. Control. Fusion **42** (2000) 1269–1289. Printed in the UK PII: S0741-3335(00)15784-7

Self-consistent equilibrium calculation through a direct variational technique in tokamak plasmas

M C R Andrade†, G O Ludwig† and S J Camargo†‡§

† Instituto Nacional de Pesquisas Espaciais, PO Box 515, 12201-970, São José dos Campos, SP, Brazil

‡ Universidade Estadual Paulista-Campus de Guaratinguetá, SP, Brazil

E-mail: mcr@plasma.inpe.br

Received 25 July 2000

Abstract. A self-consistent equilibrium calculation, valid for arbitrary aspect ratio tokamaks, is obtained through a direct variational technique that reduces the equilibrium solution, in general obtained from the 2D Grad–Shafranov equation, to a 1D problem in the radial flux coordinate ρ. The plasma current profile is supposed to have contributions of the diamagnetic, Pfirsch–Schlüter and the neoclassical ohmic and bootstrap currents. An iterative procedure is introduced into our code until the flux surface averaged toroidal current density $\langle J_T \rangle$, converges to within a specified tolerance for a given pressure profile and prescribed boundary conditions. The convergence criterion is applied between the $\langle J_T \rangle$ profile used to calculate the equilibrium through the variational procedure and the one that results from the equilibrium and given by the sum of all current components. The ohmic contribution is calculated from the neoclassical conductivity and from the self-consistently determined loop voltage in order to give the prescribed value of the total plasma current. The bootstrap current is estimated through the full matrix Hirshman–Sigmar model with the viscosity coefficients as proposed by Shaing, which are valid in all plasma collisionality regimes and arbitrary aspect ratios. The results of the self-consistent calculation are presented for the low aspect ratio tokamak *Experimento Tokamak Esférico*. A comparison among different models for the bootstrap current estimate is also performed and their possible limitations to the self-consistent calculation is analysed.

1. Introduction

The total current profile in tokamak plasmas may have contributions of several components such as the ohmic, diamagnetic and the Pfirsch–Schlüter currents, the so-called bootstrap current [1] and any other non-inductive currents that may be externally driven. An external, non-inductive current drive may be driven, for instance, radio frequency, neutral beam and helicity injections into the plasma column [2, 3], which cause a toroidal asymmetry in the system and generate a current in some privileged direction. At the moment, tokamaks work mainly as pulsed devices that are limited by the flux provided by the ohmic transformer used to sustain the plasma current. These non-inductive current drive techniques are then employed in order to enable a tokamak to operate continuously, which is important for future fusion reactor design. The bootstrap current, on the other hand, is derived from the momentum and heat flow balance equations for each species in the plasma and has its origin in neoclassical effects. High fractions of bootstrap current may be obtained in high beta poloidal equilibria and its presence

§ Present address: International Research Institute for Climate Prediction-IRI, Columbia University, PO Box 1000/61 Route 9W, Palisades, NY 10964-8000, USA.

0741-3335/00/121269+21$30.00

has already been observed in several experiments [4–6]. In advanced tokamak designs [7] and low aspect ratio configurations [8] the bootstrap current may represent a large fraction of the total plasma current, opening a new route to the viability of a steady-state reactor concept, since the generation of the total plasma current that is entirely provided by non-inductive techniques could be far more expensive. In the same way the ohmic current may be modified by neoclassical effects, since the classical Spitzer conductivity is reduced due to the presence of trapped particles. This occurs due to the toroidal tokamak geometry, which causes the trapping of circulating particles in magnetic mirrors and decreases the number of particles which can effectively carry the current. Magnetic flux consumption experiments [4–6, 9, 10] have already confirmed the prescription of neoclassical models for the plasma conductivity.

The knowledge of the total plasma current profile depends on an accurate prediction of its components and is very important for stability and transport studies in tokamak plasmas. We will consider here the first four current contributions previously mentioned: the ohmic, bootstrap, diamagnetic and Pfirsch–Schlüter currents. Non-inductive current drive and strong anisotropies in the plasma pressure profile will not be considered at the moment. The neoclassical bootstrap and ohmic currents can greatly change the total current profile but they can only be accurately determined if the total plasma current itself is known. However, the total current profile depends on the equilibrium and the equilibrium cannot be determined until all the current components have been determined, that is the total current profile is known. Therefore, we can only solve this problem with a self-consistent solution for the equilibrium. The purpose of this paper is to describe such an equilibrium for low and high aspect ratio tokamaks.

The plasma fixed boundary equilibrium is generated here from a variational principle, applied in its energy form, that uses a truncated Fourier expansion in flux coordinates (ρ, θ, ζ) to describe the magnetic surfaces in a D-shaped plasma [11]. Here ρ is the radial flux surface label, θ is the poloidal angle and ζ is the ignorable toroidal symmetry angle. Trial functions, parametrized by a set of constants that are determined by the condition of stationary energy, are introduced to represent the spectral radial amplitudes, and an approximate solution for the equilibrium is obtained through a direct variational technique. By using this Lagrangian formulation, the standard procedure of solving the 2D quasi-linear Grad–Shafranov equation, following an Eulerian approach, is reduced, in our case, to a 1D problem that consists in finding these radial coefficients.

The self-consistent calculation requires that the toroidal plasma current profile $I_T(\rho)$, used as an input to the variational procedure, takes into account all the current contributions that result from the equilibrium given in our case by the external inductive neoclassical ohmic current and the current components basically driven by pressure gradients such as the bootstrap, diamagnetic and Pfirsch–Schlüter currents [12]. In order to do this an iterative algorithm was implemented to our equilibrium calculation, where a current profile $I_T(\rho)$ is first specified, and an equilibrium is determined from the variational technique. A new $I_T(\rho)$ results from this equilibrium and is defined by the sum of the pressure-driven toroidal current components with the ohmic contribution. The flux surface average of the toroidal current density ($\langle J_T \rangle$), which is a more physically relevant profile, is then calculated for both $I_T(\rho)$ mentioned above and compared. In case they differ by more than a specified accuracy, the new $I_T(\rho)$ is reintroduced into the algorithm and a new equilibrium is calculated. Otherwise, a self-consistent solution for the equilibrium is obtained. This convergence criterion ensures that the current density profile itself is obtained consistently within the tolerance assumed for the iterative procedure. A convergence criterion applied to $f\,\mathrm{d}f/\mathrm{d}\Phi_P$ with $f(\Phi_P) = RB_T$ being the toroidal flux function, or, equivalently in our case, to $I_T(\rho)\mathrm{d}I_T/\mathrm{d}\rho$, as usually employed in self-consistent equilibrium calculations [13, 14], still leads to a self-consistent solution but the error in the convergence of $J_T(\rho, \theta)$ may be greater than that required for $I_T(\rho)\,\mathrm{d}I_T/\mathrm{d}\rho$, as will be shown

in section 4. Here, R is the distance of a given point in the plasma to the tokamak axis, B_T is the toroidal induction and Φ_P is the poloidal magnetic flux.

The bootstrap current will be determined by using the multi-species full matrix Hirshman–Sigmar model [15], with the viscosity coefficients provided according to Shaing *et al* [16], which are continuously valid throughout the three collisionality regimes (banana, plateau and Pfirsch–Schlüter regimes) arbitrary aspect ratios and for any flux surface geometry. This extends results provided by self-consistent equilibrium calculations that use more restrictive calculations for the bootstrap current estimate. We consider here the first two odd-velocity moments of the Fokker–Planck equation in order to derive the momentum and heat flux balance equations in the plasma. In high-collisional conventional tokamak plasmas, the bootstrap current effect tends to vanish since trapped particles are scattered before performing a whole excursion on their banana orbits, eliminating the neoclassical effect. However, according to Shaing *et al* [17], in the limit when the aspect ratio $A = R_0(a)/a$ tends to unity ($R_0(a)$ and a are the major and minor plasma radii, respectively) the bootstrap current is independent of the collisionality regime, and would not disappear since the ion and electron viscosities in this limit tend to infinity. We will check these prescriptions for the low aspect ratio tokamak ETE (*Experimento Tokamak Esférico*) [18], at the Associated Plasma Laboratory of the National Institute for Space Research (LAP/INPE) in Brazil, that will start operating by the end of 2000. The bootstrap current estimate will be compared to that provided using the Hirshman–Sigmar viscosity coefficients [15]. An estimate in low-collisionality regimes for the bootstrap current that is valid for arbitrary aspect ratios and which accounts for the presence of a single-ion species in the plasma (Hirshman model) [19] is also implemented in our code as an alternative to the full matrix Hirshman–Sigmar model. However the collisionless model presents some limitations to the self-consistent calculation as our code simulations will demonstrate throughout this paper.

The ohmic current is calculated in terms of the neoclassical conductivity which follows the calculation given in [20] and from the loop voltage determined such that the total plasma current $I_T(a)$ is equal to a prescribed value.

Some other neoclassical issues caused by plasma rotation [21] and orbit squeezing effects [22], characteristic of high-confinement regimes, will not be addressed at the moment. These effects can cause modifications in the neoclassical coefficients bringing the neoclassical theory into accordance with the ion transport levels observed in enhanced confinement scenarios. In the same way, corrections to the bootstrap current and to the plasma resistivity close to the magnetic axis provided by the existence of potato orbits [23] are not considered here. These corrections have to be carefully analysed according to what has been recently discussed by Helander [24].

Our self-consistent equilibrium code was implemented in a PC-type computer using the *Mathematica* package [25]. This was possible mainly because the plasma equilibrium was obtained through a semi-analytic procedure provided by the direct variational technique.

The paper is organized as follows. In section 2 we briefly present our equilibrium model and the implementation of the self-consistent calculation is described in detail. The neoclassical bootstrap and ohmic currents are introduced in section 3. In section 4 we show some results of our self-consistent equilibrium code applied to the ETE low aspect ratio tokamak. A discussion and the conclusions of the paper are presented in section 5.

2. Equilibrium model and self-consistent equilibrium formulation

As mentioned in section 1, the plasma fixed boundary equilibrium was generated through a direct variational method, applied in its energy form, that uses a spectral representation of the flux surfaces in a D-shaped plasma and trial functions to represent the radial spectral

amplitudes [11].

The truncated Fourier expansion, representing the D-shaped flux surfaces, describes the transformation from cylindrical to flux coordinates, $(R, Z) \rightarrow (\rho, \theta)$, as

$$R(\rho, \theta) = R_0(\rho) - \tfrac{1}{4}\rho T(\rho) + \rho \cos\theta + \tfrac{1}{4}\rho T(\rho) \cos 2\theta \tag{1a}$$

$$Z(\rho, \theta) = \rho E(\rho)(\sin\theta - \tfrac{1}{4} T(\rho) \sin 2\theta). \tag{1b}$$

This representation is valid for an up–down axisymmetric plasma where the toroidal ζ variable is ignored. The spectral coefficients $R_0(\rho)$, $E(\rho)$ and $T(\rho)$ represent, respectively, the centre, the elongation and the triangularity of the magnetic surfaces labelled by ρ. Appropriate trial functions are introduced for these coefficients and parametrized by a set of constants, determined from the variational technique, for a given toroidal plasma current profile $I_{\mathrm{T}}(\rho)$, pressure profiles $p(\rho)$ and prescribed boundary conditions. $I_{\mathrm{T}}(\rho)$ describes the total plasma current enclosed by a magnetic surface. Higher orders in the Fourier expansion imply more constants to be determined in the variational procedure. Once the radial amplitudes are obtained, the equilibrium calculation is complete and is reduced to the solution of a 1D problem in the radial coordinate ρ, instead of solving the 2D quasi-linear Grad–Shafranov equation in the cylindrical coordinates (R, Z). All the formalisms involving this calculation, including the construction of trial functions, are found in detail in [11].

The expression for the magnetic field in flux coordinates is given by

$$\vec{B} = \frac{1}{2\pi}(\nabla\zeta \times \nabla\Phi_{\mathrm{P}}) + \frac{\mu_0 I(\Phi_{\mathrm{P}})\nabla\zeta}{2\pi} \tag{2}$$

where the first term represents the poloidal magnetic field $\vec{B}_{\mathrm{P}}$ and the second term refers to the toroidal induction component $\vec{B}_{\mathrm{T}}$. Furthermore, Φ_{P} is the poloidal magnetic flux and $|\nabla\zeta| = 1/h_\zeta$ (h_ζ is the distance to the symmetry axis or the cylindrical coordinate R). $I(\Phi_{\mathrm{P}})$ is the total poloidal current between the symmetry axis and a given magnetic surface. This current is related to the toroidal flux function $f(\Phi_{\mathrm{p}})$ through the relation $f(\Phi_{\mathrm{p}}) = \mu_0 I(\Phi_{\mathrm{p}})/2\pi = RB_{\mathrm{T}}$.

The implementation of the self-consistent calculation of our equilibrium model will be now described.

The total current density is given in terms of four components represented by the ohmic, bootstrap, diamagnetic and Pfirsch–Schlüter currents, that is

$$\vec{J} = \frac{\langle \vec{J}_{\mathrm{oh}} \cdot \vec{B}\rangle}{\langle B^2\rangle}\vec{B} + \frac{\langle \vec{J}_{\mathrm{bs}} \cdot \vec{B}\rangle}{\langle B^2\rangle}\vec{B} + \frac{\mathrm{d}p}{\mathrm{d}\Phi_{\mathrm{P}}}\left(\mu_0 I \frac{\vec{B}}{\langle B^2\rangle} - 2\pi R^2 \nabla\zeta\right). \tag{3}$$

The first term in equation (3) is the ohmic current modified by neoclassical effects through plasma conductivity, the second term is the bootstrap current, which is calculated through the full matrix Hirshman–Sigmar model [15] with the viscosity coefficients as proposed by Shaing [16], and the last two terms are the combination of the diamagnetic and the Pfirsch–Schlüter currents ($\vec{J}_{\mathrm{dia}}$ and $\vec{J}_{\mathrm{ps}}$, respectively) [12], which are obtained from fluid plasma equations and are independent of the plasma collisionality regime. The brackets in equation (3) refer to a flux surface average, defined as

$$\langle F\rangle = \frac{\int F\,\mathrm{d}\ell_\theta/B_{\mathrm{P}}}{\int \mathrm{d}\ell_\theta/B_{\mathrm{P}}} = \frac{\int F\sqrt{g}\,\mathrm{d}\theta}{\int \sqrt{g}\,\mathrm{d}\theta} \tag{4}$$

where $\mathrm{d}\ell_\theta$ is a poloidal arc length and $\sqrt{g} = (\nabla\rho \cdot \nabla\theta \times \nabla\zeta)^{-1}$ is the Jacobian of the transformation from cylindrical (R, ϕ, Z) to flux (ρ, θ, ζ) coordinates, where $\zeta = -\phi$. The ohmic and the bootstrap currents will be presented in detail in the next section.

In order to solve the equilibrium self-consistently we need to solve the Grad–Shafranov equation taking into account equation (3).

The Grad–Shafranov equation is given by [26]

$$\Delta^* \Phi_{\mathrm{P}} = -4\pi^2 \mu_0 R^2 \frac{\mathrm{d}p}{\mathrm{d}\Phi_{\mathrm{P}}} - \mu_0^2 I \frac{\mathrm{d}I}{\mathrm{d}\Phi_{\mathrm{P}}} = 2\pi \mu_0 R J_{\mathrm{T}} \tag{5}$$

and the toroidal and poloidal current density components are described, according to Ampére's law and force balance equation, as

$$\vec{J}_{\mathrm{T}} = \left[-2\pi \mathrm{R} \frac{\mathrm{d}p}{\mathrm{d}\Phi_{\mathrm{P}}} - \frac{\mu_0 I}{2\pi R} \frac{\mathrm{d}I}{\mathrm{d}\Phi_{\mathrm{P}}} \right] \hat{e}_\zeta \tag{6}$$

$$\vec{J}_{\mathrm{P}} = -\frac{\mathrm{d}I}{\mathrm{d}\Phi_{\mathrm{P}}} \vec{B}_{\mathrm{P}} \tag{7}$$

where $\hat{e}_\zeta$ is a unit vector in the toroidal direction. The total current density which is given by the sum of equations (6) and (7) results:

$$\vec{J} = -2\pi R^2 \frac{\mathrm{d}p}{\mathrm{d}\Phi_{\mathrm{P}}} \nabla\zeta - \frac{\mathrm{d}I}{\mathrm{d}\Phi_{\mathrm{P}}} \vec{B}. \tag{8}$$

Combining equations (3) and (8), an equation for the poloidal current profile $I(\Phi_{\mathrm{p}})$ follows:

$$-I \frac{\mathrm{d}I}{\mathrm{d}\Phi_{\mathrm{P}}} = \frac{\langle \vec{J}_{\mathrm{oh}} \cdot \vec{B} \rangle}{\langle B^2 \rangle} I + \frac{\langle \vec{J}_{\mathrm{bs}} \cdot \vec{B} \rangle}{\langle B^2 \rangle} I + \frac{\mu_0 I^2}{\langle B^2 \rangle} \frac{\mathrm{d}p}{\mathrm{d}\Phi_{\mathrm{P}}}. \tag{9}$$

The self-consistent calculation implies that the toroidal current density that enters into the Grad–Shafranov equation has also to be given by the sum of all the current components as described by equation (3), that is it implies the solving of equations (5) and (9) simultaneously. Actually, in our case, instead of solving equation (5) itself we solve the equilibrium by applying variational techniques to the internal plasma energy. In fact, we solve the Grad–Shafranov equation after taking its average over a flux surface. This equation is given in [11] by

$$\frac{\mathrm{d}\Phi_{\mathrm{p}}}{\mathrm{d}\rho} \frac{\mathrm{d}}{\mathrm{d}\rho} \left(K(\rho) \frac{\mathrm{d}\Phi_{\mathrm{P}}}{\mathrm{d}\rho} \right) = -\frac{\mathrm{d}L}{\mathrm{d}\rho} I(\rho) \frac{\mathrm{d}I}{\mathrm{d}\rho} - \frac{\mathrm{d}V}{\mathrm{d}\rho} \frac{\mathrm{d}p}{\mathrm{d}\rho} \tag{10}$$

and corresponds to an extremum of the functional representing the total energy $W(a)$, given below:

$$W(a) = \iiint_{V(a)} \mathrm{d}^3 r \left(\frac{B_{\mathrm{P}}^2}{2\mu_0} + \frac{B_{\mathrm{T}}^2}{2\mu_0} + p \right) = \int_0^a \mathrm{d}\rho \, \langle H \rangle (\Phi_{\mathrm{P}}, I_{\mathrm{T}}, \rho) \tag{11}$$

where $\langle H \rangle$ is a flux surface averaged Hamiltonian density, which may be written as

$$\langle H \rangle = \frac{I_{\mathrm{T}}^2(\rho)}{2K(\rho)} + \frac{I^2(\Phi_{\mathrm{P}})}{2} \frac{\mathrm{d}L}{\mathrm{d}\rho} + p(\Phi_{\mathrm{P}}) \frac{\mathrm{d}V}{\mathrm{d}\rho}. \tag{12}$$

The three terms in equation (11) represent, respectively, the internal magnetic energy stored in the plasma loop, the internal magnetic energy stored in the plasma solenoid and the thermal energy confined in the plasma. In our Lagrangian formulation, Φ_{P} is a generalized coordinate and the toroidal plasma current profile, $I_{\mathrm{T}}(\rho)$, represents a generalized momentum given by

$$I_{\mathrm{T}}(\rho) = K(\rho) \frac{\mathrm{d}\Phi_{\mathrm{P}}}{\mathrm{d}\rho}. \tag{13}$$

$L(\rho)$, $V(\rho)$ and $K(\rho)$ are, respectively, the inductance of the toroidal solenoid coincident with a given flux surface, the volume involved by this surface and the inverse kernel used to calculate the self-inductance of the plasma loop. They depend only on the system geometry and are derived in detail in [11].

In order to complete the set of equations used in our equilibrium calculation we will introduce the internal plasma energy $U(a)$, upon which we apply the variational technique.

$U(a)$ is given by the sum of the magnetic and thermal energies, confined in the plasma, after discounting, from the total energy $W(a)$, the energy contribution due to the vacuum field. This contribution is constant for variational procedure considerations, in a fixed boundary problem, leading to an internal plasma energy written as:

$$U(a) = \int_0^a \mathrm{d}\rho \left[\frac{I_\mathrm{T}^2(\rho)}{2K(\rho)} + \frac{L(\rho)}{K(\rho)\,\mathrm{d}L/\mathrm{d}\rho} I_\mathrm{T}(\rho) \frac{\mathrm{d}I_\mathrm{T}(\rho)}{\mathrm{d}\rho} + p(\rho)\frac{\mathrm{d}V(\rho)}{\mathrm{d}\rho} + \frac{L(\rho)}{\mathrm{d}L/\mathrm{d}\rho}\frac{\mathrm{d}p(\rho)}{\mathrm{d}\rho}\frac{\mathrm{d}V(\rho)}{\mathrm{d}\rho} \right]. \tag{14}$$

The constants involved in the parametrization of the trial functions that describe the spectral coefficients of the Fourier expansion given in (1) are determined by finding a stationary value of $U(a)$, for given plasma current and pressure profiles and prescribed values of the total plasma current, $I_\mathrm{T}(a)$, pressure on the magnetic axis, $p(0)$, and at the plasma edge, $p(a)$. All the other quantities in (14) carry the geometry information of the flux surfaces. The self-consistent calculation implies that the current profile $I_\mathrm{T}(\rho)$ takes into account all current contributions, as described in (9).

The profiles $I(\rho)$ and $I_\mathrm{T}(\rho)$ are related through the following expression

$$I_\mathrm{T}(\rho)\frac{\mathrm{d}I_\mathrm{T}}{\mathrm{d}\rho} = -K(\rho)\frac{\mathrm{d}L}{\mathrm{d}\rho}I(\rho)\frac{\mathrm{d}I}{\mathrm{d}\rho} - K(\rho)\frac{\mathrm{d}V}{\mathrm{d}\rho}\frac{\mathrm{d}p}{\mathrm{d}\rho} \tag{15}$$

which results from the substitution of equation (13) into (10). Still using relation (13), we can rewrite (9) as

$$-I\frac{\mathrm{d}I}{\mathrm{d}\rho} = \frac{I_\mathrm{T}(\rho)}{K(\rho)}\left[\frac{\langle \vec{J}_\mathrm{oh}\cdot\vec{B}\rangle}{\langle B^2\rangle} I + \frac{\langle \vec{J}_\mathrm{bs}\cdot\vec{B}\rangle}{\langle B^2\rangle} I \right] + \frac{\mu_0 I^2}{\langle B^2\rangle}\frac{\mathrm{d}p}{\mathrm{d}\rho}. \tag{16}$$

In order to solve (10) and (16) simultaneously, we implemented in our code the following iterative procedure: initially, a current profile $I_\mathrm{T}(\rho)$ is specified and the equilibrium is solved by finding a stationary value for $U(a)$. From this equilibrium we obtain the profile $I\,\mathrm{d}I/\mathrm{d}\rho$ from the right-hand side of (16) and, consequently, $I_\mathrm{T}\,\mathrm{d}I_\mathrm{T}/\mathrm{d}\rho$ from (15), given by the sum of all the current components. In this way a new $I_\mathrm{T}(\rho)$ is obtained from the integration of (15). The flux surface average of the toroidal current density ($\langle J_\mathrm{T}\rangle$) is then calculated for this new profile as well as for $I_\mathrm{T}(\rho)$, previously introduced in order to generate the equilibrium. If they are different by more than a given tolerance then the new $I_\mathrm{T}(\rho)$, given by the sum of all the current components, is reintroduced into our algorithm and a new equilibrium is calculated. Otherwise a self-consistent equilibrium is obtained. A convergence criterion applied to the $I_\mathrm{T}\,\mathrm{d}I_\mathrm{T}/\mathrm{d}\rho$ or $I\,\mathrm{d}I/\mathrm{d}\rho$ profiles, as mostly used in self-consistent equilibrium codes, may result in a current density profile that is not converged to within the same accuracy as requested for $I_\mathrm{T}\,\mathrm{d}I_\mathrm{T}/\mathrm{d}\rho$, according to what will be shown in section 4.

In the next section we will present in detail the derivation for the neoclassical ohmic and bootstrap currents as introduced in our code.

3. Neoclassical ohmic and bootstrap currents

3.1. Ohmic current

The ohmic current, induced by transformer action, is solenoidal and parallel to the magnetic field and takes the following form:

$$\vec{J}_\mathrm{oh} = \frac{\langle \vec{J}_\mathrm{oh}\cdot\vec{B}\rangle}{\langle B^2\rangle}\vec{B} \tag{17}$$

or by replacing the expression for $\vec{J}_{\rm oh}$ with

$$\vec{J}_{\rm oh} = \sigma_{\rm NC} \frac{\langle \vec{E} \cdot \vec{B} \rangle}{\langle B^2 \rangle} \vec{B} \tag{18}$$

it can be written as

$$\vec{J}_{\rm oh} = \frac{\mu_0 I}{(2\pi)^2} \sigma_{\rm NC} V_{\rm loop} \frac{\langle 1/R^2 \rangle}{\langle B^2 \rangle} \vec{B}. \tag{19}$$

In (18) and (19) $\sigma_{\rm NC}$ is the plasma conductivity modified by neoclassical effects and $\vec{E}$ is the driving electric field, which is considered here to be in the toroidal direction and can be written in terms of the loop voltage $V_{\rm loop}$ as

$$\vec{E} = \frac{V_{\rm loop}}{2\pi R} \hat{e}_\zeta \tag{20}$$

where $\hat{e}_\zeta$ is the unit vector in the toroidal direction. In (19) we have also replaced the expression for the toroidal magnetic field $B_{\rm T} = \mu_0 I / 2\pi R$. $V_{\rm loop}$ is considered constant in the plasma column and is determined from the condition that the total plasma current $I_{\rm T}(a)$, given by a prescribed value, must be equal, at the same time, to the sum of all the current components, which are obtained from the integration of the respective toroidal current density over the plasma cross section:

$$I_{\rm T}(a) = I_{\rm bs} + I_{\rm oh} + I_{\rm ps} + I_{\rm dia}. \tag{21}$$

The subscripts denote, respectively, the bootstrap, ohmic, Pfirsch–Schlüter and diamagnetic currents. Once the loop voltage is determined from (21) the current profile $I\,{\rm d}I/{\rm d}\rho$, given in (16), is updated along with $I_{\rm T}(\rho)$, through (15), which will be used in the next iteration in our algorithm. The equations for all currents in (21) are given in appendix A.

The neoclassical conductivity is taken from the Hirshman–Hawryluk–Birge calculation [20], which includes modifications due to impurity species and is valid for all plasma collisionality regimes. The full expression for $\sigma_{\rm NC}$, according to this formulation, is given by

$$\frac{\sigma_{\rm NC}}{\sigma_0} = \frac{8}{3\sqrt{\pi}} \int_0^\infty x_{\rm e}^4 {\rm e}^{-x_{\rm e}^2}\, {\rm d}x_{\rm e} \{(1 - f_{\rm t}^*) F_{\rm s} [1 - f_{\rm t}^* (\nu_{\rm D}^{\rm e} \tau_{\rm ee} F_{\rm s} - 1)]\} \tag{22}$$

where $\sigma_0 = n_{\rm e} e^2 \tau_{\rm ee} / m_{\rm e}$ is the Spitzer conductivity not modified for impurities, $\tau_{\rm ee}$ is the self-scattering time between electrons given by $\tau_{\rm ee} = 12\pi^{3/2} \varepsilon_0^2 m_{\rm e}^2 v_{\rm the}^3 / (4 n_{\rm e} e^4 \ln\Lambda)$, $f_{\rm t}^*$ is an effective trapped particle fraction, $F_{\rm S}$ is the Spitzer function which can be fitted to a polynomial and $\nu_{\rm D}^{\rm e}$ is the total pitch angle diffusion frequency that depends on $x_{\rm e} = v/v_{\rm the}$, with $v_{\rm the} = (2T_{\rm e}/m_{\rm e})^{1/2}$ being the electron thermal velocity and $T_{\rm e}$ the electron temperature. The effective trapped particle fraction $f_{\rm t}^*$ is defined by $f_{\rm t}^* = f_{\rm t}[1 + 1.75 \nu*_{\rm e} (\nu_{\rm D}^{\rm e}(x_{\rm e}) \tau_{\rm ee}) x_{\rm e}^{-1}]^{-1}$, where $f_{\rm t}$ is the trapped particle fraction in the banana regime that will be introduced in the next section through (23). $\nu*_{\rm e}$ is the electron collisionality parameter given by $\nu*_{\rm e} = \sqrt{2} R_0(\rho) q(\rho) / (\tau_{\rm ee} \varepsilon^{3/2} v_{\rm the})$, where ε is the inverse of the local aspect ratio $(\rho/R_0(\rho))$ and $R_0(\rho)$ and $q(\rho)$ represent the centre and the safety factor of a given flux surface. $m_{\rm e}$, $n_{\rm e}$ and e are, respectively, the electron mass, density and electron charge. The expression for $\nu_{\rm D}^{\rm e}$ is given in appendix B and the equations for all other quantities mentioned above are given in detail in [20]. There is also an analytic form for $\sigma_{\rm NC}$, presented in [20], which gives a quite reasonable result for the plasma conductivity, including low aspect ratio tokamaks, when their approximation for the trapped particle fraction is replaced by the calculation given by Lin-Liu and Miller [27]. The accuracy of this form for the neoclassical conductivity will be shown in section 4, where it will be compared with the exact formula given by (22), indicating that it may be used in order to reduce the computer time consumption. However, in our calculations we used (22).

The next current density component to be described is the bootstrap current which is estimated in our code according to the full matrix Hirshman–Sigmar model using the viscosity coefficients as given by Shaing.

3.2. Bootstrap current

The neoclassical effect, originating from the toroidal tokamak geometry, causes the trapping of particles in magnetic mirrors that define the so-called banana orbits, which are formed in the weak magnetic field side on the outboard of the machine. The balance in the momentum exchange between the passing and trapped particles due to friction leads to a net current driven by the passing particles that is called the bootstrap current [1, 28]. This current occurs due to plasma diffusion and exists independently of any external electric field. It is, however, dependent on the existence of trapped particles in the plasma and is largest in the low-collisionality regimes (banana regime) such that the trapped particles perform a whole excursion on their orbits before being scattered, which would result in their de-trapping decreasing the bootstrap effect. In low aspect ratios, however, the bootstrap current would not disappear even in collisional plasmas, according to Shaing *et al* [17], since the ion and electron viscosities tend to infinity in this limit. We will check these assumptions in section 4.

As the trapped particle fraction f_t, is an important feature for the bootstrap current estimate, we introduce here the well known expression for f_t given by [15]

$$f_t = 1 - \frac{3}{4}\langle B^2\rangle \int_0^{1/B_{max}} \frac{\lambda\, d\lambda}{\langle\sqrt{1-\lambda B}\rangle} \tag{23}$$

where $\lambda = \sin^2\xi/B$, and ξ is the pitch angle of the particle gyro orbit. B_{max} refers to the maximum value of the total induction B, over a flux surface. An approximation to avoid calculating the integral given in (23), which actually requires a double numerical integration, is the approximation given by Lin-Liu and Miller [27], which is used in our code as described in appendix B. The accuracy of this approximation has already been checked [29] where the bootstrap current was estimated through the Hirshman collisionless model.

In analogy to the ohmic current, the bootstrap current flows parallel to the magnetic field and is divergence free, assuming the following form:

$$\vec{J}_{bs} = \frac{\langle \vec{J}_{bs}\cdot\vec{B}\rangle}{\langle B^2\rangle}\vec{B} \tag{24}$$

with

$$\langle \vec{J}_{bs}\cdot\vec{B}\rangle = \sum_a n_a e_a \langle u_{a\parallel} B\rangle \tag{25}$$

n_a e_a and $u_{a\parallel}$ are, respectively, the density, charge and parallel flow velocity of species a in the plasma.

The solution of the system consists of the parallel momentum and heat flow balance equations for each species in the plasma and provides the parallel fluid $\langle u_{a\parallel}B\rangle$ and heat $\langle 2q_{a\parallel}/5p_a\rangle$ flows in terms of the thermodynamic flows for each one of these species. q_a and p_a are, respectively, the parallel heat flow and the partial plasma pressure due to species a. The parallel fluid flows determine the bootstrap current through equation (25). Taking the flux surface averaged parallel component of the odd-velocity moments $(\vec{v}, v^2\vec{v})$ of the Fokker–Planck equation one obtains the following final expressions for the two equations mentioned above:

$$\mu_{a1}\langle u_{a\parallel}B\rangle - \mu_{a1}V_{a1}B + \frac{2}{5}\mu_{a2}\left\langle\frac{q_{a\parallel}}{p_a}B\right\rangle - \mu_{a2}V_{a2}B = \sum_b\left(l_{11}^{ab}\langle u_{b\parallel}B\rangle - \frac{2}{5}l_{12}^{ab}\left\langle\frac{q_{b\parallel}}{p_b}B\right\rangle\right) \tag{26}$$

$$\mu_{a2}\langle u_{a\parallel}B\rangle - \mu_{a2}V_{a1}B + \frac{2}{5}\mu_{a3}\left\langle\frac{q_{a\parallel}}{p_a}B\right\rangle - \mu_{a3}V_{a2}B = \sum_b\left(-l_{21}^{ab}\langle u_{b\parallel}B\rangle + \frac{2}{5}l_{22}^{ab}\left\langle\frac{q_{b\parallel}}{p_b}B\right\rangle\right) \tag{27}$$

which are derived in detail in [15]. The left-hand sides in equations (26) and (27) refer to the plasma viscosity and the right-hand sides shows the parallel friction forces acting upon a given plasma species a. The summation describing the friction forces is made over all species, including a. This system of equations is solved for the parallel flows, $\langle u_{j\parallel}B\rangle$ and $\langle q_{j\parallel}B/p_j\rangle$, and the bootstrap current is finally obtained from equation (25). V_{a1} and V_{a2} are the poloidal components of the diamagnetic flows [15], given in terms of the thermodynamic flows as

$$V_{a1} = -\frac{\mu_0 I T_a}{e_a B}\left(\frac{1}{p_a}\frac{\mathrm{d}p_a}{\mathrm{d}\Phi_\mathrm{P}} + \frac{e_a}{T_a}\frac{\mathrm{d}\phi}{\mathrm{d}\Phi_\mathrm{P}}\right) \tag{28}$$

$$V_{a2} = -\frac{\mu_0 I T_a}{e_a B}\left(\frac{1}{T_a}\frac{\mathrm{d}T_a}{\mathrm{d}\Phi_\mathrm{P}}\right). \tag{29}$$

In equations (28) and (29), T_a is the temperature of species a. The electric potential ϕ is the same for all species and does not contribute to the final bootstrap current estimate.

In order to complete this formulation and have all the elements to solve the system of equations established by equations (26) and (27), we have to define the viscosity (μ_{aj}) and friction (l_{ij}^{ab}) coefficients. The latter relate the friction forces experienced by the plasma species in terms of the parallel flows and are given in appendix B. They are independent of the magnetic field and so are valid in all neoclassical collision frequency regimes.

The viscosity coefficients for each species, on the other hand, depend on the plasma collisionality and are used here according to Shaing *et al*'s formulation, see [16, 30]:

$$\left\{\begin{array}{c}\mu_{a1}\\ \mu_{a2}\\ \mu_{a3}\end{array}\right\} = \frac{8}{3\sqrt{\pi}}n_a m_a\int_0^\infty \mathrm{d}x_a\, x_a^4\,\mathrm{e}^{-x_a^2}\left\{\begin{array}{c}1\\ (x_a^2-5/2)\\ (x_a^2-5/2)^2\end{array}\right\}\frac{K_\mathrm{B}^a K_\mathrm{PS}^a}{K_\mathrm{B}^a + K_\mathrm{PS}^a}. \tag{30}$$

These coefficients are valid throughout the three plasma collisionality regimes and arbitrary aspect ratios, with K_B and K_PS being the banana and Pfirsch–Schlüter contributions to the viscosity integral, respectively given by

$$K_\mathrm{B}^a = \frac{f_\mathrm{t}}{f_\mathrm{c}}\nu_\mathrm{D}^a \tag{31}$$

and

$$K_\mathrm{PS}^a = \frac{3}{2}v_{\mathrm{th}a}^2 x_a^2\sum_{m=1}^\infty F_m\frac{(\nu_\mathrm{T}I_R^m)_a}{\nu_\mathrm{T}^a}. \tag{32}$$

In equation (32) we have

$$F_m = \frac{2}{\langle B^2\rangle\langle\vec{B}\cdot\nabla\theta\rangle}\langle\sin m\Theta(\hat{n}\cdot\nabla B)\rangle\langle\sin m\Theta(\vec{B}\cdot\nabla\Theta)(\hat{n}\cdot\nabla B)\rangle \tag{33}$$

and

$$(\nu_\mathrm{T}I_R^m)_a = -\frac{3}{2}\left(\frac{\nu_\mathrm{T}^a}{\omega_{m,a}}\right)^2 - \frac{9}{2}\left(\frac{\nu_\mathrm{T}^a}{\omega_{m,a}}\right)^4 + \left\{\frac{1}{4} + \left[\frac{3}{2} + \frac{9}{4}\left(\frac{\nu_\mathrm{T}^a}{\omega_{m,a}}\right)^2\right]\left(\frac{\nu_\mathrm{T}^a}{\omega_{m,a}}\right)^2\right\} \times\frac{2\nu_\mathrm{T}^a}{\omega_{m,a}}\arctan\left(\frac{\omega_{m,a}}{\nu_\mathrm{T}^a}\right) \tag{34}$$

with $\Theta = \gamma(\Phi_\mathrm{P})\int_0^\ell B\,\mathrm{d}\ell_\theta/B_\mathrm{P}$, $1/\gamma(\Phi_\mathrm{P}) = 1/(2\pi)\oint B\,\mathrm{d}\ell_\theta/B_\mathrm{P}$ and $\hat{n} = \vec{B}/B$. $\omega_{m,a} = x_a v_{\mathrm{th}a} m(\vec{n}\cdot\nabla\Theta)$, where $x_a = v/v_{\mathrm{th}a}$, with $v_{\mathrm{th}a}$ being the thermal velocity for species a. We

Table 1. Parameters of the tokamak ETE.

Major radius $R_0(a)$	0.30 m
Minor radius a	0.20 m
Triangularity δ	0.3
Toroidal magnetic field on axis B_0	0.4 T
Plasma current $I_T(a)$	200 kA

have not considered the $\cos m\Theta$ terms in F_m since we are dealing with up–down symmetric plasmas where these terms do not contribute. Still, in equation (31) we have f_t and $f_c = 1 - f_t$ representing, respectively, the trapped and circulating particle fractions. The definitions for the collision frequencies ν_D^a and ν_T^a in (31) and (32) are given in appendix B.

The number of modes to be used in the summation of equation (32) can be estimated employing the identity:

$$\sum_{m=1}^{\infty} F_m = \frac{\langle(\hat{n}\cdot\nabla\vec{B})^2\rangle}{\langle B^2\rangle}. \tag{35}$$

These expressions for the viscosity coefficients provide an estimate for the bootstrap current valid in all collisionality regimes and arbitrary aspect ratios. They were derived using an approximation for the Coulomb collision operator and their accuracy is within 20% of those calculated from the full form of this collision operator as already mentioned in [15, 16, 30]. The estimate of the bootstrap current will be compared to those obtained from the Hirshman–Sigmar model [15] that, in spite of being valid in all collisionality regimes, does not give the right limit when the aspect ratio tends to unity and to the Hirshman model [19], valid for all aspect ratios in low-collisionality regimes.

4. Applications

We will present some results of the self-consistent equilibrium calculation for the ETE low aspect ratio tokamak [18]. Its main parameters are summarized in table 1.

The plasma beta during the ohmic phase is expected to be between 4 and 10%. The pressure, electron and ion temperature profiles, used in the self-consistent calculation, were taken as Gaussian-shaped functions in the following form: $f(\rho) = f(0)\exp[-\alpha_f(\rho/(w_f - \rho))^2]$. The parameter $f(0)$ determines the profile value at the axis, whereas α_f and w_f control the gradient and the width of the profile, and, therefore, the value at the boundary. We have also considered $T_e(0) = T_i(0)$, $T_e(a) = T_i(a)$ and $\alpha_{T_e} = \alpha_{T_i}$. As the pressure profile is given as a fixed input in our code, the density profiles were derived by taking into account the fact that the total pressure in the plasma is given by $p = n_e T_e + \sum_k n_k T_k$ and considering the quasi-neutrality condition ($n_e = \sum_k n_k Z_k$), with the summations taken over all ion species.

The initial current profile $I_T(\rho)$, first specified in the variational procedure, is taken as given in [11] with an amplitude $A_0 = 1/5$, its centre at $\rho_0 = 0$ and a width $w = 2a/3$, with a being the minor plasma radius. α_I is the initial peaking factor current profile. We have established a tolerance of 1% for $\langle J_T\rangle$ in the self-consistent calculation in most of the equilibria analysed.

In table 2 we show the estimate of the bootstrap current fraction $I_{bs}/I_T(a)$, resulting from the self-consistent equilibrium, according to the full matrix Hirshman–Sigmar model [15] with the viscosity coefficients given by Shaing *et al* [16]. Different plasma parameters were considered, such as the pressure on the magnetic axis $p(0)$, the central electron and ion temperatures $T_{e,i}(0)$, the peaking factor pressure profile (α_p), the elongation at the plasma

Table 2. Plasma parameters for bootstrap current estimate in ETE generated from the self-consistent calculation.

	$p(0)$ (kPa)	$T_{e,i}(0)$(keV)	$T_{e,i}(a)$(keV)	α_p	$\alpha_{T_{e,i}}$	$\kappa(a)$	Z_{eff}	β_I	β_0	$I_{bs}/I_T(a)$
I	15	0.5	0.03	3.0	0.2	2.0	1.54	0.54	0.09	0.36
II	10	0.4	0.03	3.0	0.2	2.0	1.00	0.36	0.06	0.23
III	10	0.4	0.03	3.0	0.2	2.0	1.54	0.36	0.06	0.22
IV	10	0.2	0.03	3.0	0.2	2.0	1.00	0.36	0.06	0.14
V	10	0.4	0.03	3.0	0.2	1.7	1.00	0.31	0.06	0.17
VI	10	0.4	0.03	2.0	0.2	2.0	1.00	0.39	0.06	0.24
VII	8	0.4	0.03	3.0	0.2	2.0	1.00	0.29	0.05	0.18

edge $\kappa(a)$ and the level of impurities in the plasma where $Z_{eff} = 1$ corresponds to a pure hydrogen plasma and $Z_{eff} = 1.54$ represents a hydrogen plasma plus 2% carbon. Z_{eff} was considered constant over the plasma column. The optimum case, represented by the set of parameters I, with a central pressure of 15 kPa and a plasma elongation of $k(a) = 2.0$, gives a bootstrap current fraction of approximately 36% and poloidal beta $\beta_I = 0.54$, where $\beta_I = 4 \int p \, dV/(\mu_0 R_m I_T^2(a))$, as in [13], with R_m being the radius of the magnetic axis. Comparing cases II and V let us conclude that more elongated plasmas correspond to higher bootstrap current fractions. These plasmas have higher safety factors generating more bootstrap current according to equation (A.5), see appendix A. Plasmas with 2% carbon, as in case III, present a slight decrease in the bootstrap current as observed from a comparison with II. We can also confirm from the set of parameters I, II and V that the bootstrap current fraction generated in the plasma is proportional to the β_I values [28, 31]. Although the final combination of parameters may result in the same β_I , as in II, III and IV, the bootstrap current level is more or less sensitive to some plasma profile parameters and may be different in each of these cases. The low temperature in case IV, for instance, is the main cause of the low bootstrap current obtained due to the increase on the plasma collisionality. Finally, flatter pressure profiles produce a slightly higher bootstrap current fraction, as observed by comparing II and VI, and generate current closer to the plasma edge, which can be destabilizing. β_0 in table 2 refers to the toroidal beta calculated with the external magnetic field at the geometric centre. The plasma parameters presented in table 2 represent ETE plasmas in ETE's first phase of operation, when no additional heating is predicted, making higher levels of bootstrap current unlikely. Calculations with our code for other machines, such as MAST [32] or NSTX [33], reproduce bootstrap current fractions that can reach more than 50%, since these machines will be able to operate with more elongated plasmas at higher temperature levels.

Figure 1 shows the current density profiles for cases II (figures 1(a)–(c)) and IV (figures 1(d)–(f)) that result from the self-consistent equilibrium. For case II, the plasma temperature is higher ($T_e(0) = 0.4$ keV) and fewer collision occur than in IV. In figures 1(a) and 1(d), the full curves refer to the total equilibrium current density profile, whereas the dashed curves are the ohmic contributions, the dash–dotted curves are the sum of the diamagnetic and Pfirsch–Schlüter currents and the dotted curves represent the bootstrap current components. Figures 1(b) and 1(e) show the consistency of the solution since the full curve correspond to the final equilibrium current densities used as input to the variational procedure and the dashed curves refer to the sums of the toroidal current contributions (ohmic, bootstrap, diamagnetic and Pfirsch–Schlüter currents) obtained from the equilibrium. Finally, the flux surface average of the total parallel equilibrium current and its ohmic and bootstrap contributions are plotted in figures 1(c) and 1(f) (note that the Pfirsch–Schlüter and diamagnetic components are null). The dashed curves are the ohmic currents, determined from the differences between the equilibrium

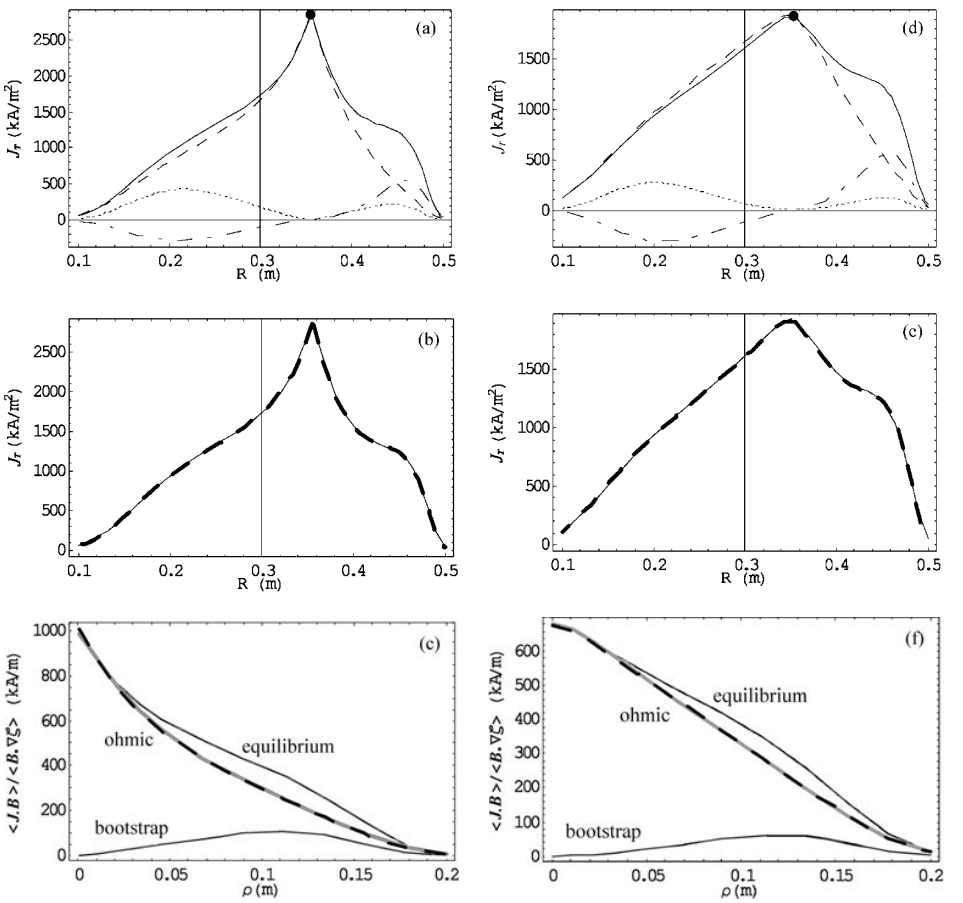

Figure 1. Toroidal current density profile components are shown in (a) and (d) for cases II and IV of table 2, respectively. The full curves correspond to the total equilibrium currents, the dashed curves refer to the ohmic components, the dash-dotted curves show the sum of the diamagnetic and Pfirsch–Schlüter contributions and the dotted curves refer to the bootstrap currents. (b) and (e) show the current density profiles obtained from the final $I_T(\rho)$ used in the variational procedure (full curve) and the sum of all current density contributions provided by the equilibrium solution (dashed curves). Finally, the parallel equilibrium current density and its ohmic and bootstrap contributions are plotted in (c) and (f). The grey curves are the ohmic currents provided by the loop voltage and neoclassical conductivity and the dashed curves are the differences between the total equilibrium and the bootstrap current components.

and the bootstrap currents, whereas the grey curves refer to the ohmic currents obtained from the plasma conductivities and the loop voltages obtained self-consistently, showing, once more, the consistent solution that results from our equilibrium calculation. The vertical lines in these figures correspond to the tokamak geometric centre and the full points refer to the magnetic axis.

The peaked current density observed for case II ($T_e(0) = 0.4$ keV), in figures 1(a) and 1(b), follows the behaviour of the neoclassical conductivity, which is reduced in relation to the Spitzer conductivity (already corrected for impurities), as shown in figure 2(a). This reduction increases the loop voltage, and the sharpness of the neoclassical conductivity decreases the

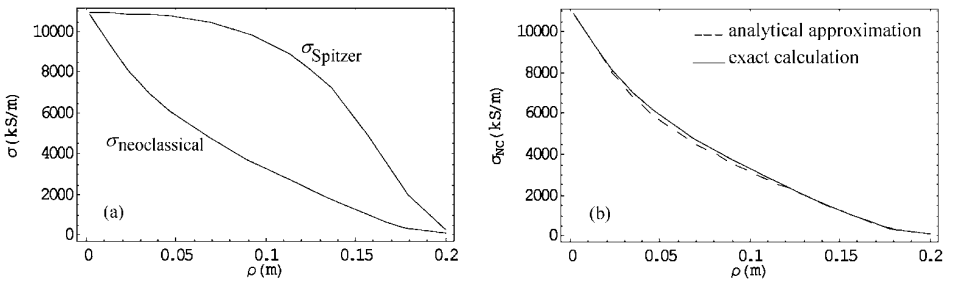

Figure 2. Neoclassical conductivity reduction in relation to the Spitzer conductivity corrected for impurities for case II (a) and a comparison between the full form of $\sigma_{\rm NC}$, given in equation (22), (full curve) and the analytical approximation proposed in [20] (dashed curve) (b).

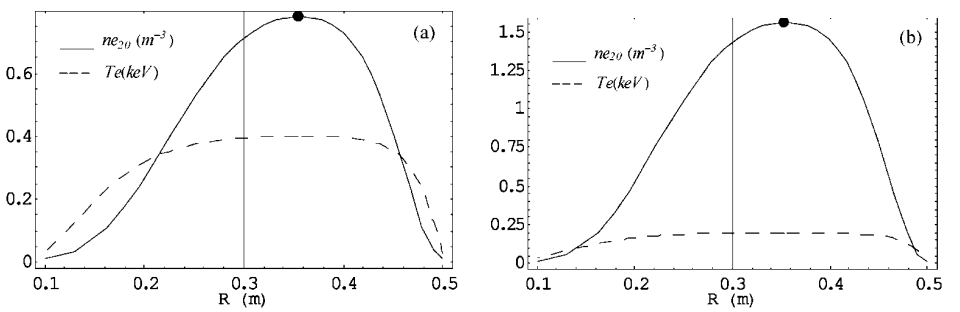

Figure 3. Temperature and density profiles for the set of parameters II (a) and IV (b) of table 2.

safety factor at the magnetic axis in relation to the classical equilibrium. Near the magnetic axis ($\rho = 0$), where the neoclassical effects are diminished since the trapped particle fraction tends to zero, both values of the conductivity coincide according to the usual neoclassical theory. Corrections to the trapped particle fraction close to the magnetic axis, due to potato orbit effects [23], might bring modifications to the bootstrap current and to the neoclassical conductivity in this region, which could lead to a different profile behaviour around $\rho = 0$. However, these corrections have to be carefully analysed as discussed in [24]. Figure 2(b) shows a comparison for $\sigma_{\rm NC}$ obtained from equation (22) and from the analytical form given in [20] for the set of parameters II. In the analytical calculation we used the trapped particle fraction according to the Lin-Liu and Miller approximation [27]. The figure shows that the analytical calculation is quite reasonable and may be used in order to speed up the computer calculations.

Typical temperature and density profiles used in the self-consistent calculation are shown in figures 3(a) and 3(b) for cases II and IV, respectively. As the pressure profiles are the same and kept constant in both cases, higher temperatures lead to lower density values and *vice versa*.

In table 3 we have all the current component contributions for the sets of plasma parameters I, II and V, in table 2, with the respective safety factors at the plasma centre and in the plasma edge, and the loop voltage $V_{\rm loop}$ that results from the self-consistent calculation. From table 3 we notice that as the bootstrap current increases, following the behaviour of the poloidal beta (β_I), the inductive ohmic current decreases, decreasing the required loop voltage and so the magnetic flux consumption. At the same time, the safety factor increases on the magnetic axis as the bootstrap current fraction increases.

Table 3. Plasma parameters and contributions to the total plasma current provided by the self-consistent calculation for cases I, II and V in table 2.

	$I_T(a)$ (kA)	I_{bs} (kA)	I_{dia} (kA)	I_{ps} (kA)	I_{oh} (kA)	$q(0)$	$q(a)$	β_I	V_{loop} (V)
I	200	71.9	12.2	−2.74	119	0.92	9.25	0.54	0.41
II	200	45.7	8.26	−1.78	148	0.71	9.11	0.36	0.57
V	200	34.8	7.91	−1.61	159	0.52	6.99	0.31	0.76

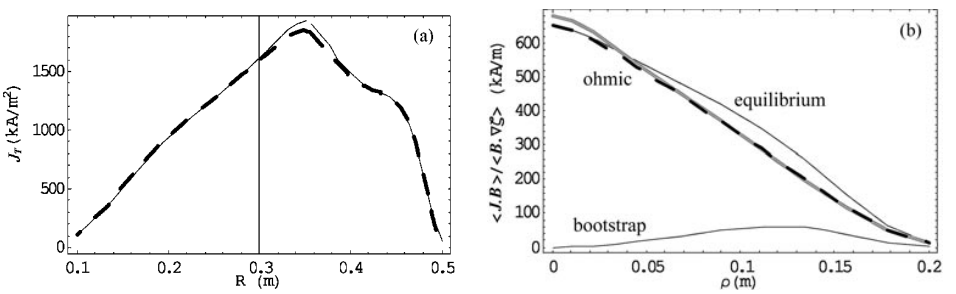

Figure 4. Same profiles shown in figures 1(e) and 1(f) for case IV, with the convergence criterion applied to $I_T dI_T/d\rho$ and not to $\langle J_T \rangle$.

Figure 4 shows the same set of profiles as given in figures 1(e) and 1(f), for case IV, obtained here by requiring the convergence of $I_T dI_T/d\rho$ instead of applying the convergence criterion to the flux surface average of the toroidal current density profile $\langle J_T \rangle$ as used in figures 1(e) and 1(f). From figures 4(a) and 4(b) we can note that although a tolerance of 1% was adopted for the convergence of $I_T dI_T/d\rho$, the error observed in the convergence of the current density profiles is amplified. Only for an extremely low tolerance in the convergence of the $I_T dI_T/d\rho$, the current density J_T will converge in the same way as shown in figures 1(e) and 1(f).

The bootstrap current profiles obtained from different models are plotted for comparison in figure 5 for the sets of parameters II and IV. The full curves represent the full matrix Hirshman–Sigmar model with the viscosity coefficients as given by Shaing *et al* and presented in section 3.2. The dashed curves refer to the Hirshman–Sigmar model with the viscosity matrix coefficients K_{ij}^a, taken from the Hirshman–Sigmar [15], corrected by a $1/f_c$ factor in order to reproduce the correct limit in the finite aspect ratio banana regime (f_c is the fraction of circulating particles in the plasma). Finally, the dash–dotted curves refer to the collisionless Hirshman model. In both cases the model that uses the Hirshman–Sigmar viscosity coefficients overestimates the bootstrap current in a rate that is higher for more collisional plasmas (figure 5(b)). As the plasma collisionality decreases, the results provided by the Hirshman–Sigmar and Shaing *et al* models approach each other, since the viscosity coefficients derived by Shaing *et al* tend to the Hirshman–Sigmar coefficients in the banana regime when these are corrected by the $1/f_c$ factor mentioned above. We can also observe that the bootstrap current reduction due to the plasma collisionality is important even in low aspect ratios ($A \leqslant 2$). Our simulations for the NSTX, considering an aspect ratio of the order 1.25, shows that the suppression of the bootstrap current due to the plasma collisionality still takes place, confirming results provided by [30]. We pushed limits down to $A = 1.15$ and could still observe the bootstrap current reduction in the collisional regimes. Checking Shaing *et al*'s assumptions at ultra-low aspect ratios with $A \to 1$ is more difficult to carry out since a set of realistic plasma parameters has first to be found and so far we do not know of any feasible

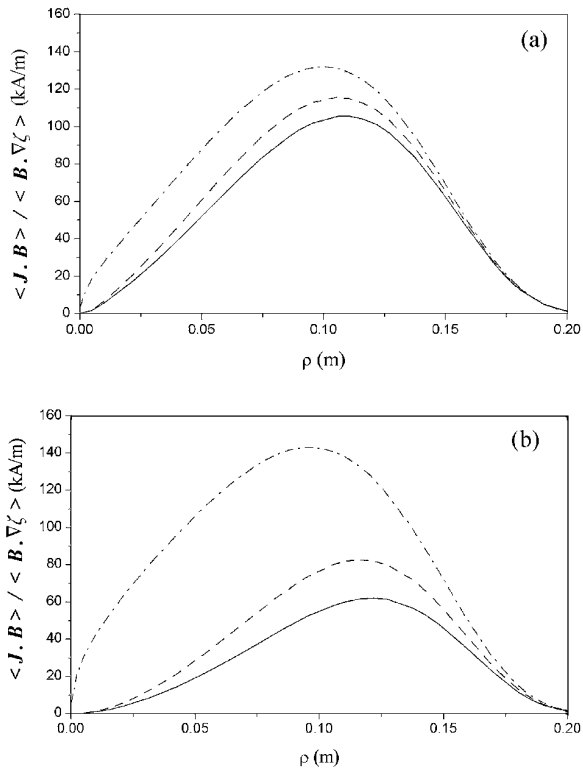

Figure 5. Bootstrap current profiles provided by different models for cases II (a) and IV (b) in table 2. The full curves refer to the Hirshman–Sigmar matrix formulation with the viscosity coefficients derived by Shaing *et al* , the dashed curves refer to the Hirshman–Sigmar model, and the dash–dotted curves refer to the collisionless Hirshman model.

device proposal at this limit. The plasmas shown here are not collisional close to the plasma edge because we have considered a very low pressure on the plasma border. The Hirshman collisionless model provides the highest bootstrap current estimate. This occurs since it does not take into account the particles scattering due to collisions, which would modify the plasma viscosity and decrease the bootstrap effect.

For the same reason, self-consistent equilibrium calculations, where the bootstrap current estimate is performed with the Hirshman collisionless model, may provide unusual current profiles close to the magnetic axis (when the plasma goes into the plateau regime). This problem is more pronounced in more collisional plasmas, as we could expect. Figure 6 illustrates this fact, showing the toroidal current profiles for cases II (figure 6(a)) and IV (figure 6(b)), of table 2. We can see that for case IV, more collisional, the current profile presents an unusual behaviour close to the magnetic axis, in relation to that shown in figure 1(d) and obtained by using the Hirshman–Sigmar full matrix form and the viscosity coefficients given by Shaing *et al*. For the plasma parameters described in II the problem is less pronounced, although the bootstrap current is still overestimated by the Hirshman collisionless model.

The parallel fluid fluxes $\langle u_{a\parallel} B \rangle$ for case III and for a plasma corresponding to the same set of parameters as given in IV, but with 2% carbon, are illustrated in figure 7 in arbitrary

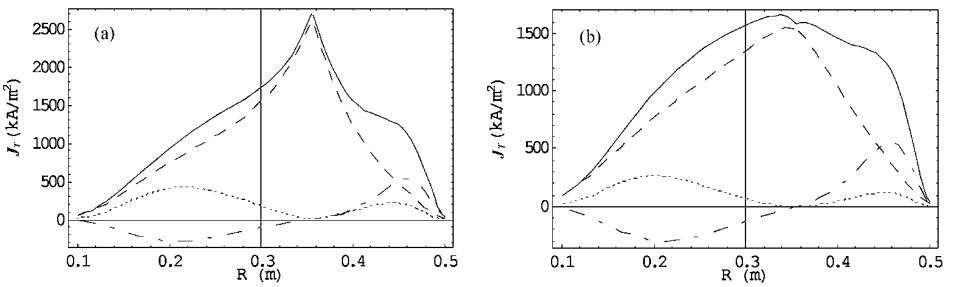

Figure 6. Toroidal current density profiles as shown in figures 1(a) and 1(d), with the bootstrap current provided by the Hirshman collisionless model.

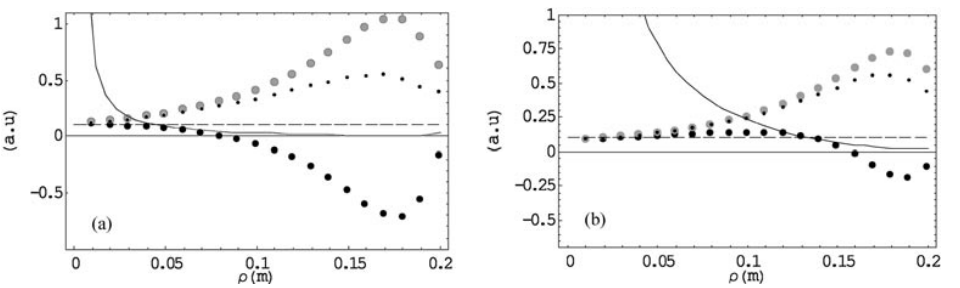

Figure 7. Normalized parallel fluid fluxes $\langle u_{\|a} B \rangle$ for cases III (a) and IV +2% carbon (b). The grey circles correspond to the hydrogen fluid flux, the large full circles to the electron population and the small full circles to the carbon fluid flux. The full curves refer to the normalized flux surface averaged collisionality parameter $\bar{\nu}_{*a}$. When a dashed curve crosses a full curve the collisionality parameter is equal to one.

units. The large full circles refer to the electron population, the large grey circles refer to the hydrogen ions and the small full circles refer to the carbon ion population. The full curves are the normalized flux surface averaged collisionality parameter $\bar{\nu}_{*e}$, given in appendix B, and the point where the dashed curves cross the full curves refer to a collisionality parameter equal to one. Therefore, the plasma regions where the collisionalities are below these curves are in the banana regime. We can see that for case IV, +2% carbon (figure 7(b)), this occurs only in a small region of the plasma column. We notice that all the fluid fluxes tend to travel in the same direction until the plasma collisionality decreases to below the banana limit, when the electron and ion fluxes will tend to travel in opposite directions. The sooner this happens, that is the less collisional is the plasma, the higher will be the bootstrap current fraction. The fluid fluxes are normalized by the same factor in figures 7(a) and 7(b).

5. Summary and conclusions

We have presented a self-consistent equilibrium calculation for low and high aspect ratio tokamak plasmas where the fixed boundary equilibrium is generated through a direct variational technique that uses a truncated Fourier expansion to represent the flux surfaces in a D-shaped plasma. The direct variational technique is applied in its energy form and consists in finding the radial coefficients of this spectral representation that are determined from the condition of stationary energy. In this way, the plasma equilibrium, in general obtained from the solution

of the 2D quasi-linear Grad–Shafranov equation, is reduced to a 1D problem in the radial flux coordinate ρ. The self-consistent calculation, implemented in our equilibrium code, requires that the toroidal plasma current profile $I_T(\rho)$, used as an input to the variational technique, takes into account the contributions that result from the equilibrium corresponding to the diamagnetic, Pfirsch–Schlüter and the neoclassical bootstrap and ohmic currents. The convergence criterion used in the self-consistent calculation is applied to the flux surface average of the toroidal current density $\langle J_T \rangle$, rather than to the current profile $I_T(\rho)$ itself or to the toroidal flux function $f(\Phi_P) = RB_T$, as usually employed in self-consistent equilibrium codes. This is due to the fact that the error allowed for the convergence of $I_T dI_T/d\rho$ might be amplified when looking at the current density profile, that is the current density profile might not be converged to within the same accuracy as that requested for $I_T dI_T/d\rho$.

The bootstrap current profile is obtained from the Hirshman–Sigmar full matrix formulation with the viscosity coefficients as given by Shaing *et al* . These coefficients are valid in all collisionality regimes and arbitrary aspect ratios. This estimate is compared to those provided by the Hirshman–Sigmar and the Hirshman collisionless models. We could observe that both Hirshman–Sigmar and the Hirshman models overestimate the bootstrap current when compared to the formulation employed in this paper. It is interesting to note that the bootstrap current does suffer a reduction in collisional regimes, even when evaluated by the Hirshman–Sigmar/Shaing *et al* formulation, for low aspect ratio machines as is the case of the ETE tokamak. As the collisionality decreases, the bootstrap current profiles provided by the Hirshman–Sigmar/Shaing *et al* and the Hirshman–Sigmar formulations approach each other. Still regarding the different calculations available for the bootstrap current estimate, we note that the Hirshman collisionless model may lead to unusual current density profiles close to the magnetic axis. The problem is more pronounced for collisional plasmas, as expected. This occurs since this model does not properly take into account the plasma viscosity in this region. The bootstrap current for the ETE tokamak may roughly represent 10–35% of the total plasma current in its first phase of operation depending on the plasma profile parameter optimization. More elongated plasmas provide higher fractions of the bootstrap current and the presence of impurities cause a slight decrease in the bootstrap contribution.

The ohmic current is calculated in terms of the neoclassical conductivity and from the loop voltage obtained from the self-consistent calculation, requiring that the total plasma current has a prescribed value that must be equal, at the same time, to the sum of all the toroidal current components. Peaked density profiles for plasmas of higher temperatures follow the behaviour of the neoclassical conductivity, which is reduced in relation to the Spitzer conductivity, already corrected for impurities. Potato orbits close to the magnetic axis, not considered in the present work, might change the current profile behaviour in this region due to corrections to the trapped particle fraction and could result in different profiles for the bootstrap current and for the plasma conductivity. However, according to [24], the bootstrap current would still be very small around the magnetic axis. As already pointed out in the introduction of this paper, plasma rotation and orbit squeezing effects, characteristic of high-confinement regimes, were not taken into account and will be considered in future works. As a next step it would be interesting to implement the faster bootstrap current evaluation provided by the fitted formula given in [34] in order to speed up the calculation of the bootstrap current and compare the results obtained with the Hirshman–Sigmar/Shaing *et al* model. This fitted formula is valid throughout all of the collisionality regimes and arbitrary aspect ratios and uses the full Coulomb collision operator (rather than an approximated one), increasing the accuracy of the viscosity coefficients by 20% in relation to those used in this paper. On the other hand, it does not consider the effects of potato orbit close to the magnetic axis and has an approximated form of dealing with impurities in the plasma. Finally, in the banana regime, the Coulomb collision

operator could be used as given by Taguchi in [35].

Acknowledgments

The first author would like to thank Dr H R Wilson from Culham Laboratoy, UK, and J G Ferreira from INPE for useful discussions on this work. We also thank the partial financial support of Ministério da Ciência e Tecnologia-MCT through its grant programme PCI and Fundação de Amparo à Pesquisa do Estado de São Paulo-FAPESP.

Appendix A

The total toroidal bootstrap, ohmic, diamagnetic and Pfirsch–Schlüter currents that are used in the loop voltage calculation (equation (21)) and that may be compared to the plasma current $I_T(a)$ are obtained by integrating the respective toroidal current density component over the plasma cross section. Starting, for instance, with the bootstrap current, we have

$$I_{bs} = \int J_{bsT}(\rho,\theta)\frac{\sqrt{g}}{h_\zeta}\,d\rho\,d\theta. \tag{A.1}$$

Recalling equation (24) we have the fact that the toroidal component of the bootstrap current density is given by

$$J_{bsT} = \frac{\langle \vec{J}_{bs}\cdot\vec{B}\rangle}{\langle B^2\rangle}B_T. \tag{A.2}$$

Replacing (A.2) into (A.1) and taking the equation for the toroidal magnetic field, we obtain

$$I_{bs} = \frac{\mu_0}{2\pi}\int_0^a d\rho\frac{\langle \vec{J}_{bs}\cdot\vec{B}\rangle}{\langle B^2\rangle}I(\rho)\int_0^{2\pi}\frac{\sqrt{g}}{h_\zeta^2}\,d\theta. \tag{A.3}$$

Using the expression for the inductance of the toroidal solenoid coincident with a flux surface [11], $L(\rho) = \mu_0/2\pi\int\sqrt{g}/h_\zeta^2\,d\rho\,d\theta$, and its derivative with respect to the radial coordinate, we may rewrite (A.3) as

$$I_{bs} = \int_0^a d\rho\frac{\langle \vec{J}_{bs}\cdot\vec{B}\rangle}{\langle B^2\rangle}I(\rho)\frac{dL}{d\rho}. \tag{A.4}$$

Finally, in terms of the safety factor profile ($q(\rho)$), given by $q(\rho) = K(\rho)I(\rho)/I_T(\rho)(dL(\rho)/d\rho)$ [11], the total toroidal bootstrap current may be written as

$$I_{bs} = \int_0^a d\rho\frac{I_T(\rho)}{K(\rho)}q(\rho)\frac{\langle \vec{J}_{bs}\cdot\vec{B}\rangle}{\langle B^2\rangle}. \tag{A.5}$$

In analogy to the toroidal bootstrap current given by equation (A.5), the total toroidal ohmic current is also given by

$$I_{oh} = \int_0^a d\rho\frac{\langle \vec{J}_{oh}\cdot\vec{B}\rangle}{\langle B^2\rangle}I(\rho)\frac{dL}{d\rho} = \frac{\mu_0}{(2\pi)^2}V_{loop}\int_0^a \sigma_{NC}I^2(\rho)\frac{\langle 1/R^2\rangle}{\langle B^2\rangle}\frac{dL}{d\rho}\,d\rho \tag{A.6}$$

and may be written in terms of the $q(\rho)$ profile similarly to (A.5).

The toroidal diamagnetic and Pfirsch–Schlüter currents are obtained from the integration, over the plasma cross section, of the toroidal component of the third and fourth terms in equation (3), leading to

$$I_{(dia+ps)} = \int\frac{K(\rho)}{I_T(\rho)}\frac{dp}{d\rho}\left(\mu_0 I\frac{B_T}{\langle B^2\rangle} - 2\pi h_\zeta\right)\frac{\sqrt{g}}{h_\zeta}\,d\rho\,d\theta \tag{A.7}$$

or, in terms of the inductance $L(\rho)$, and the volume $V(\rho) = 2\pi \int \sqrt{g}\, \mathrm{d}\rho\, \mathrm{d}\theta$:

$$I_{(\mathrm{dia+ps})} = \int_0^a \frac{K(\rho)}{I_\mathrm{T}(\rho)} \frac{\mathrm{d}p}{\mathrm{d}\rho} \left(\frac{\mu_0 I^2}{\langle B^2 \rangle} \frac{\mathrm{d}L}{\mathrm{d}\rho} - \frac{\mathrm{d}V}{\mathrm{d}\rho} \right) \mathrm{d}\rho. \tag{A.8}$$

Appendix B

B.1. Friction coefficients

The friction coefficients, used in the description of the friction forces in the momentum balance equations (26) and (27), are defined as:

$$l_{ij}^{ab} = \left(\sum_k \frac{n_a m_a}{\tau_{ak}} M_{ak}^{i-1,j-1} \right) \delta_{ab} + \frac{n_a m_a}{\tau_{ab}} N_{ab}^{i-1,j-1} \tag{B.1}$$

where the element matrices $M_{ab}^{i,j}$ and $N_{ab}^{i,j}$ are given below:

$$M_{ab}^{00} = -\left(1 + \frac{m_a}{m_b}\right)(1 + x_{ab}^2)^{-3/2} = -N_{ab}^{00} \tag{B.2}$$

$$M_{ab}^{01} = -\frac{3}{2}\left(1 + \frac{m_a}{m_b}\right)(1 + x_{ab}^2)^{-5/2} = -N_{ab}^{10} \tag{B.3}$$

$$M_{ab}^{11} = -\left(\frac{13}{4} + 4x_{ab}^2 + \frac{15}{2}x_{ab}^4\right)(1 + x_{ab}^2)^{-5/2} \tag{B.4}$$

$$N_{ab}^{11} = \frac{27}{4}\frac{T_a}{T_b} x_{ab}^2 (1 + x_{ab}^2)^{-5/2} \tag{B.5}$$

with δ_{ab} being the Kronecker delta. We may also make use of the following relations:

$$M_{ab}^{ij} = M_{ab}^{ji} \tag{B.6}$$

$$N_{ab}^{ij} = \frac{T_a}{T_b}\frac{v_{\mathrm{th}a}}{v_{\mathrm{th}b}} N_{ba}^{ji}. \tag{B.7}$$

The summation in equation (B.1) is made over all species, including a. However, it will only be evaluated when $a = b$. Still, in equation (B.1), $\tau_{ab} = 12\pi^{3/2}\varepsilon_0^2 m_a^2 v_{\mathrm{th}a}^3/(4n_b Z_b^2 Z_a^2 e^4 \ln\Lambda)$ is the collision time between species a and b, m_a is the mass of species a, e is the electron charge and $\ln\Lambda$ is the Coulomb logarithm. $x_{ab} = v_{\mathrm{th}b}/v_{\mathrm{th}a}$, with $v_{\mathrm{th}a} = \sqrt{2T_a/m_a}$ being the thermal velocity of species a and T_a is the temperature related to species a.

B.2. Collision frequencies

The collision frequencies used in (31) and (32) are given by

$$\nu_\mathrm{D}^a(v) = \frac{3\sqrt{\pi}}{4} \sum_b \frac{1}{\tau_{ab}} \left(\frac{\Phi(x_a/x_{ab}) - G(x_a/x_{ab})}{x_a^3} \right) \tag{B.8}$$

$$\nu_\mathrm{T}^a(v) = \frac{3\sqrt{\pi}}{4} \sum_b \frac{1}{\tau_{ab}} \left[\left(\frac{\Phi(x_a/x_{ab}) - 3G(x_a/x_{ab})}{x_a^3} \right) + 4\left(\frac{T_a}{T_b} + \frac{1}{x_{ab}^2} \right) \frac{G(x_a/x_{ab})}{x_a} \right] \tag{B.9}$$

where $\Phi(x)$ is the error function and $G(x) = [\Phi(x) - x\Phi'(x)]/(2x^2)$ is the Chandrasekhar function. The summations in (B.8) and (B.9) are made over all species, including a.

The flux surface averaged collisionality parameter, shown in figure 7, is defined as

$$\bar{\nu}_*^a(v) = \frac{8 f_\mathrm{t} \omega_{\mathrm{T}a} \langle B^2 \rangle 1}{3\pi v_{\mathrm{th}a}^2 \langle (\hat{n} \cdot \nabla B)^2 \rangle \tau_{aa}} \tag{B.10}$$

where f_t is the trapped particle fraction, τ_{aa} is given in appendix A, ω_{Ta} is the transit frequency ($\omega_{Ta} = v_{tha}/L_c^*$) and L_c^* is the connection length, which represents the distance along the field line from the inside to the outside of the torus. It is given by [15]:

$$L_c^* = \langle B^2\rangle^2 \langle (\hat{n}\cdot\nabla B)^2\rangle^{-1} \langle \vec{B}\cdot\nabla\theta\rangle^{-1} \sum_k \frac{2}{k} \langle \sin k\Theta (\hat{n}\cdot\nabla B)/B\rangle \langle \sin k\Theta (\hat{n}\cdot\nabla B)/B^2\rangle \quad \text{(B.11)}$$

with $\Theta = \gamma(\Phi_P)\int_0^\ell B\,\mathrm{d}\ell_\theta/B_P$ and $1/\gamma(\Phi_P) = 1/(2\pi)\oint B\,\mathrm{d}\ell_\theta/B_P$.

The trapped particle fraction was calculated according to the Lin-Liu and Miller formulation [27], considering the lower and upper approximations to the full integral given by equation (23):

$$f_{tlow} = 1 - \langle B^2\rangle \left\langle B^{-2}\left[1 - \left(1 - \frac{B}{B_{max}}\right)^{1/2}\left(1 + \frac{B}{2B_{max}}\right)\right]\right\rangle \quad \text{(B.12)}$$

$$f_{tup} = 1 - \frac{\langle B^2\rangle}{\langle B\rangle^2}\left[1 - \left(1 - \frac{\langle B\rangle}{B_{max}}\right)^{1/2}\left(1 + \frac{\langle B\rangle}{2B_{max}}\right)\right] \quad \text{(B.13)}$$

and, finally,

$$f_t = 0.75 f_{tup} + 0.25 f_{tlow}. \quad \text{(B.14)}$$

References

[1] Bickerton R J, Connor J W and Taylor J B 1971 *Nature Phys. Sci.* **229** 110
[2] Fisch N J 1987 *Rev. Mod. Phys.* **59** 175
[3] Jarboe T R *et al* 1998 *Phys. Plasmas* **5** 1807
[4] Zarnstorff M C *et al* 1988 *Phys. Rev. Lett.* **60** 1306
[5] Challis C D *et al* 1989 *Nucl. Fusion* **29** 563
[6] Kikuchi M *et al* 1990 *Nucl. Fusion* **30** 343
[7] Kessel C *et al* 1994 *Phys. Rev. Lett.* **72** 1212
[8] Peng Y-K M 2000 *Phys. Plasmas* **7** 1681
[9] Zarnstorff M C *et al* 1990 *Phys. Fluids* B **2** 1852
[10] Ward D J 1994 *Plasma Phys. Control. Fusion* **36** 673
[11] Ludwig G O 1997 *Plasma Phys. Control. Fusion* **39** 2021
[12] Hazeltine R D and Meiss J D 1991 *Plasma Confinement* (New York: Addison) vol 86
[13] Tokuda S, Takeda T and Okamoto M 1989 *J. Phys. Soc. Japan* **58** 871
[14] Wilson H R 1994 *Report* UKAEA FUS 271
[15] Hirshman S P and Sigmar D J 1981 *Nucl. Fusion* **21** 1079
[16] Shaing K C *et al* 1996 *Phys. Plasmas* **3** 965
[17] Shaing K C *et al* 1995 *Phys. Plasmas* **2** 349
[18] Del Bosco E *et al* 1998 *Proc. 4th Int. Workshop on Spherical Torus (Tokyo, October, 1998)*
[19] Hirshman S P 1988 *Phys. Fluids* **31** 3150
[20] Hirshman S P, Hawryluk R J and Birge B 1977 *Nucl. Fusion* **17** 611
[21] Helander P 1998 *Phys. Plasmas* **5** 1209
[22] Shaing K C, Hsu C T and Hazeltine R D 1994 *Phys. Plasmas* **1** 3365
[23] Shaing K C, Hazeltine R D and Zarnstorff M C 1997 *Phys. Plasmas* **4** 1371
[24] Helander P 2000 *Phys. Plasmas* **7** 2878
[25] Wolfram S 1996 *The Mathematica Book* 3rd edn (Cambridge: Wolfram Media–Cambridge University Press)
[26] Shafranov V D 1958 *Sov. Phys.–JETP* **6** 545
[27] Lin-Liu Y R and Miller R L 1995 *Phys. Plasmas* **2** 1666
[28] Kessel C E 1994 *Nucl. Fusion* **34** 1221
[29] Andrade M C R and Ludwig G O 1997 *Plasma Phys. Control. Fusion* **39** 1041
[30] Houlberg W A *et al* 1997 *Phys. Plasmas* **4** 3230
[31] Pomphrey N 1992 *Report* PPPL-2854 Princeton Plasma Physics Laboratory, Princeton, NJ
[32] Morris A W *et al* 1998 *Proc. 1st IAEA Technical Committee Meeting on Spherical Tori (Tokyo, 1998)* ed M Katsurai and Y Takase p 194 (available from the University of Tokyo)

[33] Kaye S *et al* 1999 *Fusion Technology* **36** 16
[34] Sauter O, Angioni C and Lin-Liu Y R 1999 *Phys. Plasmas* **6** 2834
[35] Taguchi M 1988 *Plasma Phys. Control. Fusion* **30** 1897